Journal of ELECTRONIC MATERIALS, Vol. 46, No. 2, 2017
DOI: 10.1007/s11664-016-4972-9

Ag/Ni Metallization Bilayer: A Functional Layer for Highly Efficient Polycrystalline SnSe Thermoelectric Modules

SANG HYUN PARK,[1] YOUNGHWAN JIN,[1,2] KYUNGHAN AHN,[3] IN CHUNG,[3,4,5] and CHUNG-YUL YOO[1,6]

1.—Advanced Materials and Devices Laboratory, Korea Institute of Energy Research, 152 Gajeong-ro, Yuseong-gu, Daejeon 34129, Republic of Korea. 2.—Department of Physics, Chungnam National University, 99 Daehak-ro, Yuseong-gu, Daejeon 34134, Republic of Korea. 3.—School of Chemical and Biological Engineering and Institute of Chemical Processes, Seoul National University, Seoul 08826, Republic of Korea. 4.—Center for Nanoparticle Research, Institute for Basic Science (IBS), Seoul 08826, Republic of Korea. 5.—e-mail: inchung@snu.ac.kr. 6.—e-mail: cyoo@kier.re.kr

The structural and electrical characteristics of Ag/Ni bilayer metallization on polycrystalline thermoelectric SnSe were investigated. Two difficulties with thermoelectric SnSe metallization were identified for Ag and Ni single layers: Sn diffusion into the Ag metallization layer and unexpected cracks in the Ni metallization layer. The proposed Ag/Ni bilayer was prepared by hot-pressing, demonstrating successful metallization on the SnSe surface without interfacial cracks or elemental penetration into the metallization layer. Structural analysis revealed that the Ni layer reacts with SnSe, forming several crystalline phases during metallization that are beneficial for reducing contact resistance. Detailed investigation of the Ni/SnSe interface layer confirms columnar Ni-Sn intermetallic phases [(Ni_3Sn and Ni_3Sn_2) and $Ni_{5.63}SnSe_2$] that suppress Sn diffusion into the Ag layer. Electrical specific-contact resistivity ($5.32 \times 10^{-4}\ \Omega\ cm^2$) of the Ag/Ni bilayer requires further modification for development of high-efficiency polycrystalline SnSe thermoelectric modules.

Key words: Thermoelectric, SnSe, interfaces, contact resistivity

INTRODUCTION

A thermoelectric module is a well-known device that can convert thermal energy to electrical energy from waste heat sites like those in industrial incinerators, automobiles, and the steel industry. The average power conversion efficiency of thermoelectric modules has remained less than 5% for several decades.[1–4] However, in recent years, exploration of novel thermoelectric materials has opened up new possibilities for highly efficient thermoelectric technology.[5–7] Rogl et al. reported *n*-type skutterudites that had a high Figure of Merit (*ZT:* 1.8) with an optimum fraction of In filler.[8] The Yamamoto group reported high-performance nanostructured PbTe-based material with $ZT \sim 1.8$ at 810 K for *p*-type PbTe.[9] In their work, the Yamamoto group also demonstrated a PbTe thermoelectric module with maximum conversion efficiency of 11% for a temperature difference of 590 K. Zhao reported a maximum *ZT* of 0.964 for Sb0.5%-Zn0.5% doped Mg_2Si at 880 K.[10] Among these high-performance thermoelectric materials, SnSe is getting particular attention for its world-record high figure of merit ($ZT \sim 2.6$) results.[11] Since the first report of the world's highest *ZT* result with a SnSe material in 2014, many research groups have started to pursue development of the high-performance thermoelectric modules with SnSe. Unlike other well-known high-temperature thermoelectric materials such as PbTe or skutterudite, there are very few reported studies of metallization structures or module fabrication steps with the thermoelectric SnSe material. As

(Received July 5, 2016; accepted September 16, 2016; published online October 6, 2016)

depicted in Fig. 1, a thermoelectric module consists of both *n*- and *p*-type thermoelectric legs, and electrodes that electrically connect these legs in series. To develop high-efficiency thermoelectric modules, minimization of the contact resistivity between the thermoelectric materials and metallic parts is one of the most important technological issues.[12] The detailed structural illustration in Fig. 1 shows that the metallic parts are composed of electrodes, brazing fillers, and metallization layers. The formation of the metallization layers on both ends of the thermoelectric legs, in particular, contributes to the overall internal resistance of the thermoelectric module.

In this work, the formation of metallization layers on SnSe employing an Ag/Ni bilayer was investigated to overcome the drawbacks of Ag and Ni used separately. Successful Ag-based metallization with a Ni functional layer could be applied with improved electrical contact resistivity (5.32×10^{-4} Ω cm^2).

EXPERIMENTAL

Stoichiometric amounts of elemental Sn and Se were weighed for the synthesis of SnSe and loaded into a fused silica tube. The tube was flame-sealed under a vacuum of $\sim 1.33 \times 10^{-3}$ Pa. The tube was then heated to 950°C during 12 h, held at the same temperature for 24 h, and then passively cooled in the furnace. The ingot obtained from the furnace reaction was placed in a glove box and ground mechanically, after which the ground powder was sieved. The powder particles under 45 μm were processed *via* spark plasma sintering (SPS, Fuji Electronic Industrial Co., Ltd. SPS-211LX) with 40 MPa pressure at 510°C for 5 min. To make an Ag or Ni metallized surface on the SnSe, Ag or Ni layers were prepared by employing 200 mesh Ag powder (≥99.99%, Sigma-Aldrich), Ag pellets (prepared from 200 mesh Ag powder), or 200 mesh Ni powder (≥99.99%, Sigma-Aldrich) on top and bottom of the 2-mm thick SnSe inside a graphite mold (Ø = 12 mm). Then, it was hot-pressed at 15 MPa and 650°C in a vacuum. To apply the Ag/Ni metallization bilayer, 0.4 g of Ag and 0.03 g of Ni were pressed together to prepare Ag/Ni pellets, and then stacked on both sides of the SnSe. This was followed by vacuum hot pressing under the same conditions of Ag metallization. These ingots were processed to form rectangular thermoelectric legs using a diamond wheel saw and wire saw, as shown in Fig. 2a and b.

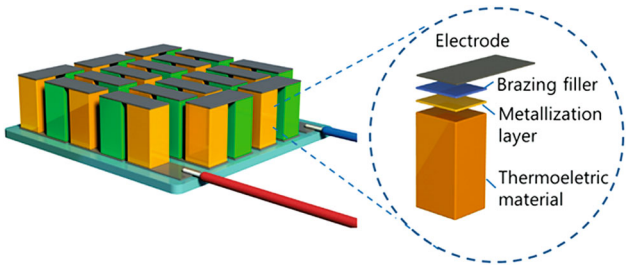

Fig. 1. Schematics of a thermoelectric module and detailed structure of thermoelectric-leg bonding layers.

Microstructural analyses were conducted using scanning electron microscopy (SEM, JEOL JSM-7000F) to investigate the characteristics of the interface between the SnSe and the metallization layer. Energy dispersive spectroscopy (EDS) line-scan analyses were also conducted to analyze the distribution of each element at the metallization layer interface. A compositional and phase investigation of the metallization interface after the high-temperature hot-press was carried out, using x-ray photoelectron spectroscopy (XPS, Thermo VG Scientific, K-alpha) and x-ray diffraction measurements (XRD, Rigaku, D/MAX-2500). The contact resistivity between the SnSe and metallization layers was measured using the in-house resistance scanning measurement apparatus presented in Ref. 13.

RESULTS AND DISCUSSION

Among various candidate metal layers that might be used to form the thermoelectric material interface, Ag was utilized due to its cost effectiveness in both powder and foil forms.[14–16] Thus, in this work, the interfacial characteristics of Ag metallization on SnSe were investigated using two different types of Ag-powder-based metallization processes. First, bare Ag powder was located directly on both sides of the SnSe pellet and co-sintered at 15 MPa and 650°C in a vacuum. A secondary Ag pellet-type metallization sample was prepared using cold-pressed Ag pellets that were located on both sides of the SnSe under the same sintering conditions. The cross-section views of the surfaces of both Ag powder and Ag pellet metallization layers are shown in Fig. 2a and b. In both cases, the Ag metallization layers are bonded robustly to the SnSe thermoelectric leg surface without interfacial cracks or delamination. Figure 2c shows contact resistivity characteristics of 7.03 mΩ cm^2 for the Ag powder metallized leg, and 3.75 mΩ cm^2 for the Ag pellet metallized leg. These two different processed Ag metallization showed very similar and relatively high contact resistivity characteristics. EDS line scanning of these two metallized thermoelectric legs showed unexpected Sn distribution inside the Ag metallization layer, while Se showed no penetration. The solid white scanning line of Sn in Fig. 2d and e clearly showed a relatively higher profile than the Se distribution into the Ag layer side. This Sn diffusion at the metallization interface indicates that more Sn could diffuse into the Ag side when an Ag-metallized SnSe thermoelectric module is used for long-term power generation at high temperature. Even though the Ag metallization made a robust metallized layer on the SnSe thermoelectric legs, the Sn diffusion into the Ag metallized layer could significantly deteriorate the long-term reliability of the metallization interface for thermoelectric modules. The results in Fig. 2 clearly show that

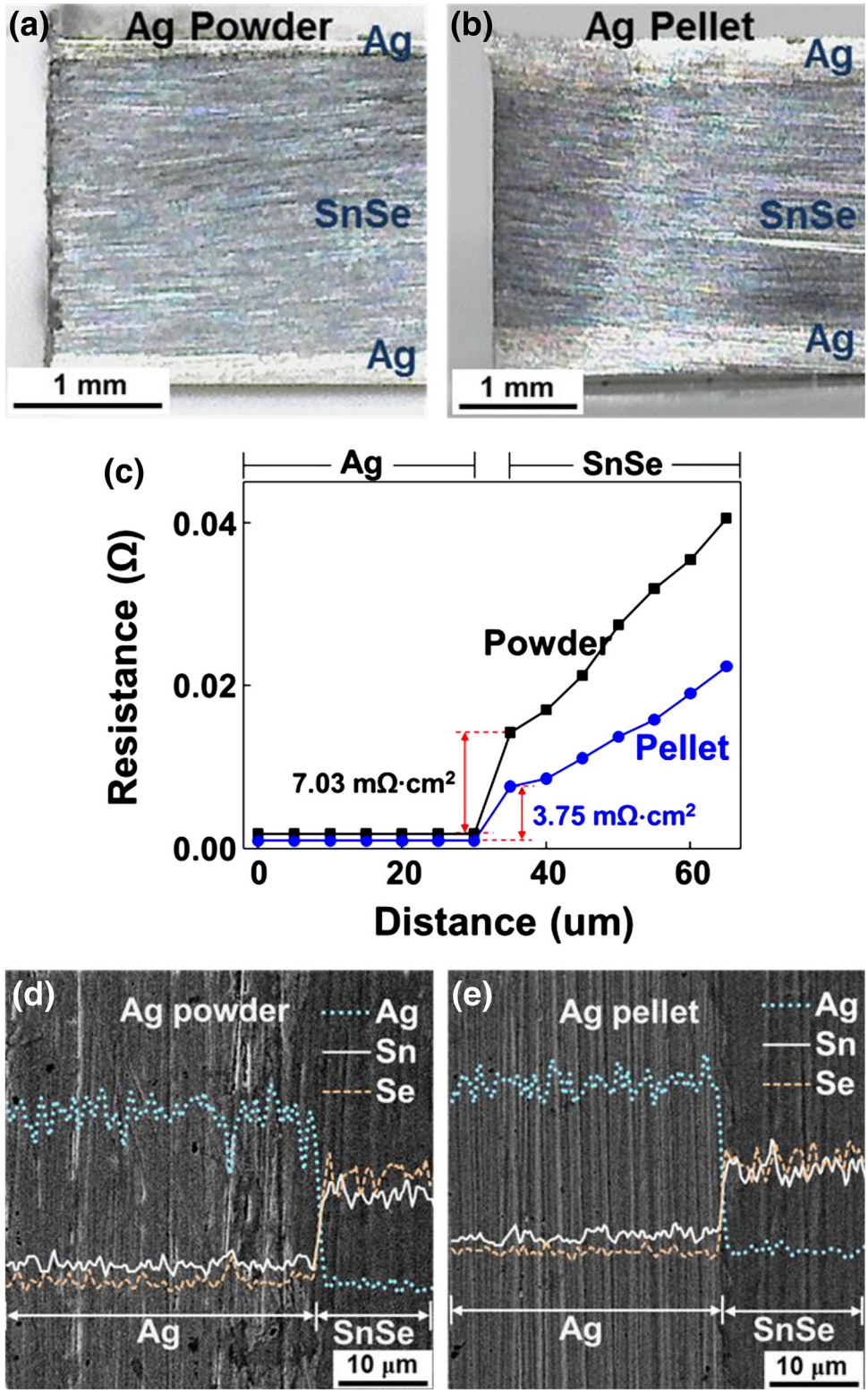

Fig. 2. (a) Photographs of polycrystalline SnSe thermoelectric legs metallized with (a) Ag powder and (b) Ag pellet, (c) Specific-contact resistivity comparison from the resistance scanning results. SEM and EDS element line scanning results of (d) Ag powder and (e) Ag pellet metallized SnSe thermoelectric legs.

a single Ag layer is not likely to make a reliable metallization interface for a SnSe thermoelectric leg.

Ni layers are known to form effective barriers to elemental diffusion,[17–20] and thus might be useful to prevent Sn diffusion into the metallization layer.

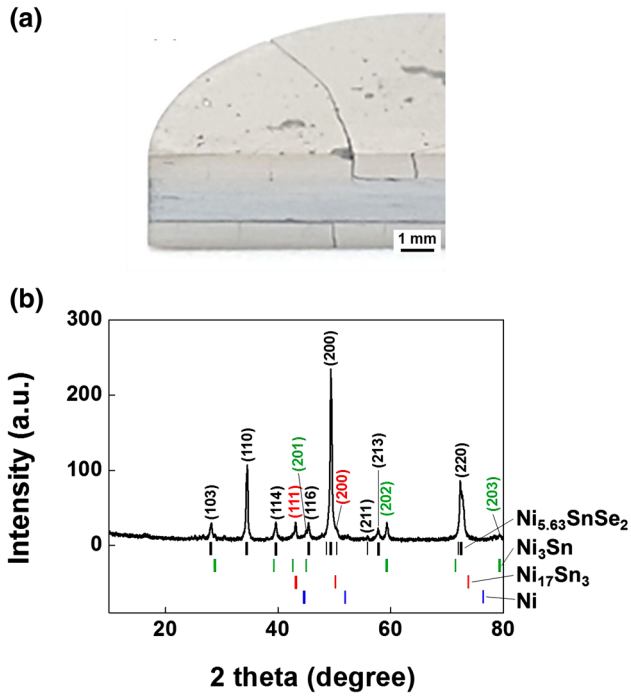

Fig. 3. (a) Photograph of surficial and interfacial cracks of single Ni layer metallization on polycrystalline SnSe, and (b) XRD phase analysis of the Ni metallization layer.

Hard and ductile nickel is one of the best corrosion-resistant metals, because an oxide layer naturally forms on its surface. For this reason, it has been widely utilized as a coating metal. An investigation of a single Ni metallization layer on SnSe was done, and the results are shown in Fig. 3. The Ni-powder metallization shows that direct Ni metallization on SnSe results in severe crack formation as shown in Fig. 3a. An XRD pattern of the Ni metallization layer in Fig. 3b shows that the whole Ni powder layer reacted with SnSe during the metallization process, and that the resultant layer was composed of $Ni_{5.63}SnSe_2$, $Ni_{17}Sn_3$, and Ni_3Sn, as indexed in Fig. 3b. The cracks in the metallization layer in Fig. 3a could be induced by the difference in thermal expansion coefficients of SnSe and one of the Ni-Sn intermetallic phases detected in Fig. 3b. Based on the formation of such cracks, it is unlikely that a single Ni metallization layer could establish robust contact with the SnSe thermoelectric leg.

To alleviate Sn penetration into the Ag metallization layer as well as the interfacial cracking during Ni metallization, an Ag/Ni bilayer metallization structure is proposed. To fabricate this Ag/Ni metallization bilayer, 0.4 g of Ag and 0.03 g of Ni were pressed together to prepare Ag/Ni pellets, and then stacked on both sides of the SnSe pellet with the Ni layers facing the SnSe surfaces, as shown in the inset of Fig. 4a. The multi-stacked pellets were sintered by vacuum hot pressing under the same conditions of Ag metallization. It was demonstrated that Ag/Ni bilayer metallization showed no cracks or delamination after hot-pressing. The EDS line scanning result in Fig. 4a showed no significant Sn penetration into the Ag layer compared to the Sn profile in Fig. 2d and e. Introduction of the Ni interlayer significantly suppressed Sn diffusion into the Ag layer. Detailed investigation by EDS shows that the Ni layer formed two distinguishable layers (marked 1st and 2nd Ni layer) after metallization via vacuum hot press sintering. The 1st Ni layer shows Ni, Sn, and Se elemental distribution, while the 2nd Ni layer shows Ni and Sn with suppressed Se distribution. When the Ni reacts with SnSe at the Ni/SnSe interface during the hot-pressing, excess Ni reacts first with SnSe to form $Ni_{5.63}SnSe_2$ together with Sn ($SnSe \xrightarrow{\text{excess Ni}} Ni_{5.63}SnSe_2 + Sn$) to compose the first Ni layer. Then, the remnant Sn reacts with excess Ni further to form Ni-Sn intermetallic phases (Ni_3Sn and Ni_3Sn_2) to form the second Ni layer, in the partial presence of $Ni_{5.63}SnSe_2$.

The resultant contact resistivity of this Ag/Ni bilayer metallization was measured (5.32×10^{-4} Ω cm^2) and is shown in Fig. 4b. The changeover of the different resistivity (ρ_1 and ρ_2) is also found, as visualized in the resistance scanning results in Fig. 4b. The two different resistivity ranges coincide with the two distinguishable EDS element distributions, as marked with yellow dashed lines in Fig. 4a and b. This coincidence between EDS element scanning and resistance scanning clearly proved that the Ni layer resulted in two distinguishable layers with different electrical characteristics. Detailed investigation of the contact resistance characteristics in Fig. 4b explains that the interface between SnSe and the metallic layer (2nd Ni layer) makes electrical specific-contact resistivity so low that it could barely be noticed in the resistance line scanning. In this result from investigation of the Ag/Ni bilayer, the most distinct and large specific-contact resistivity came from the interface of two different metallic layers (the Ag and 1st Ni layer). Normally, the biggest specific-contact resistivity would be expected to be located at the interface between the metallization layer and thermoelectric material (SnSe in this case) because these two materials have different characters (metal and semiconductor). In this work, it was found that in metallization cases involving formation of multi-layer structures as the result of metallization, the term “overall specific-contact resistivity” would be preferred, to distinguish this situation from that described by the previous (common) term “specific-contact resistivity”. The latter condition is confined to the contact resistivity right at the interface between the metallization layer and thermoelectric material.

Compared to the Ag single metallization investigation in Fig. 2c, which showed significant contact resistivity at the SnSe and metal layer interface, the Ag/Ni bilayer structure showed almost tenfold lower

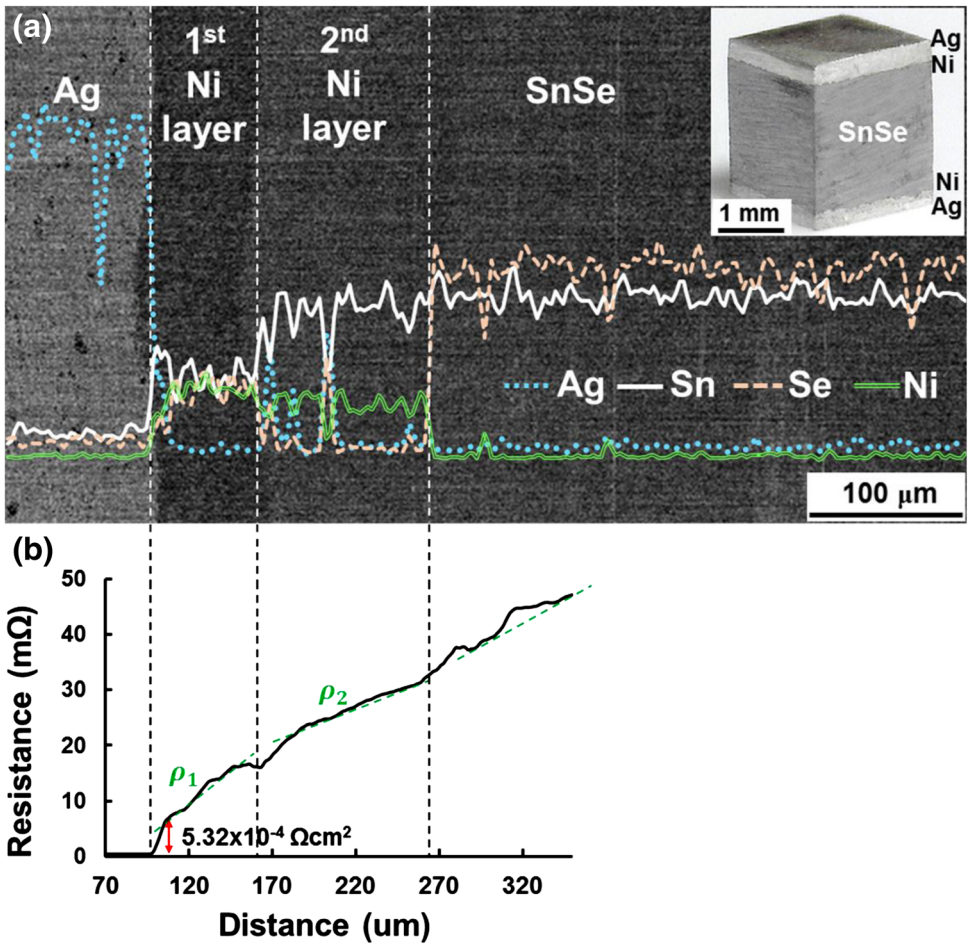

Fig. 4. (a) SEM and EDS line scanning investigations (Inset: Photograph of the Ag-Ni bilayer SnSe thermoelectric leg) of Ag/Ni bilayer metallization on SnSe, and (b) Specific-contact resistivity from the resistance line scanning result.

electrical contact resistivity between the thermoelectric SnSe and metallic layer. This contact resistivity difference could be caused by Sn penetration into the Ag layer, as shown in Fig. 2d and e. Pure metal generally shows lower electrical resistivity than alloyed metal; consequently, unalloyed Ag in the Ag/Ni/SnSe layer could induce lower contact resistivity compared to Sn alloyed Ag in the Ag/SnSe layer. However, based on the electrical contact resistivity of 5.32×10^{-4} Ω cm^2 with Ag/Ni bilayer metallization, further modification is necessary compared to previously reported PbTe or skutterudite cases that showed a contact resistivity range as low as 10^{-5} Ω cm^2.[21–23] The slightly high electrical specific-contact resistivity of the Ag/Ni bilayer on polycrystalline SnSe could be caused by the relatively low electrical conductivity of SnSe.[11] The room temperature electrical conductivity reported by the Kanatzidis group was around 0.1 to 10^2 S cm^{-1}, which is quite lower than that of Half-Heusler and skutterudite.[24,25] Polycrystalline SnSe in this work also showed a low electrical conductivity of ~2 S cm^{-1}. Further investigations on improving the electrical contact resistivity as well as the electrical conductivity of polycrystalline SnSe should be conducted to develop highly efficient SnSe thermoelectric modules.

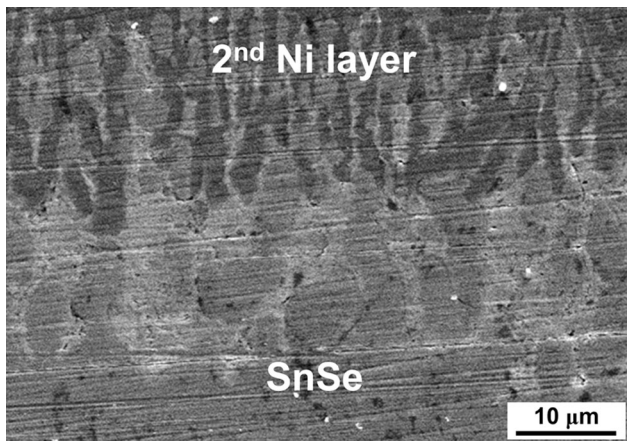

Fig. 5. SEM microstructural analysis of the Ag/Ni bilayer metallization interface.

Further modification of the interface between the two different metallic layers could be easier, or have

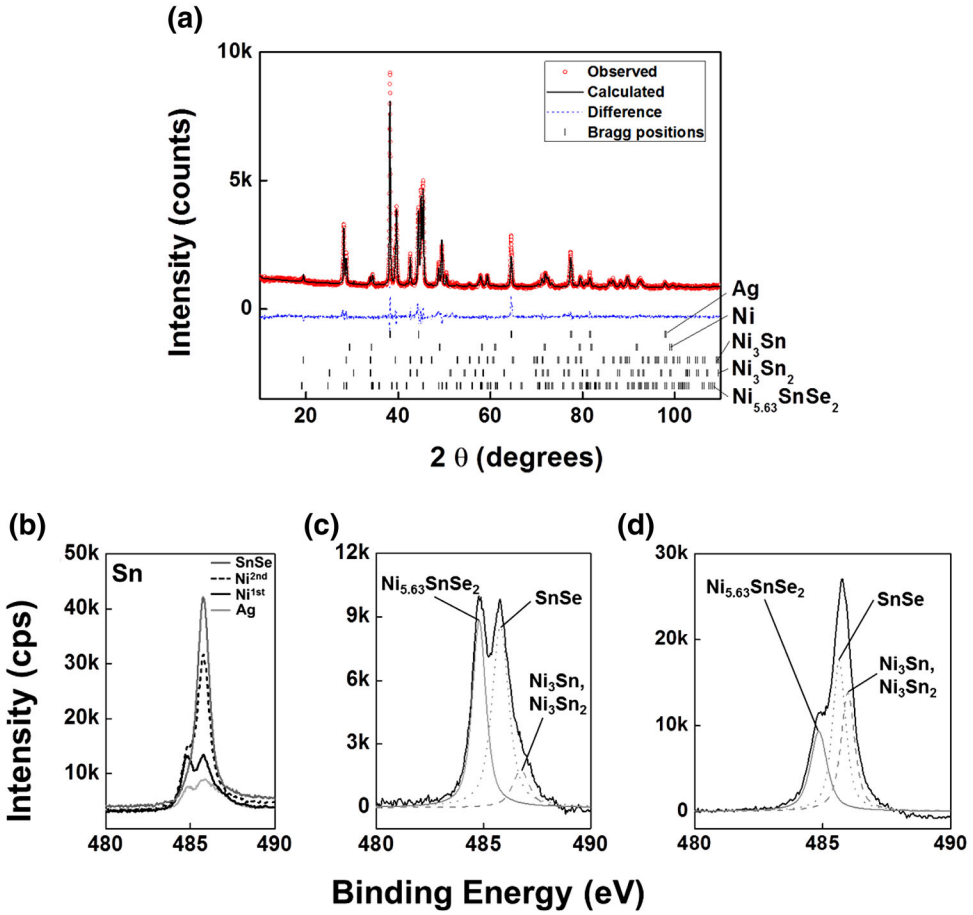

Fig. 6. (a) Rietveld refinement result for XRD pattern: observed (red open circles), calculated (black line), and difference (blue line) of Ag, Ni and SnSe powder after sintering at 650°C in a vacuum with 15 MPa. Bragg positions of cubic Ag (space group: $Fm\bar{3}m$, lattice parameter: a = 4.089 (1) Å), cubic Ni (space group: $Fm\bar{3}m$, lattice parameter: a = 3.520 (1) Å), hexagonal Ni_3Sn (space group: $P6_3/mmc$, lattice parameter: a = 5.298 (1) Å and c = 4.251 (1) Å), hexagonal Ni_3Sn_2 [space group: $P6_3/mmc$, lattice parameter: a = 4.119 (1) Å and c = 5.289 (1) Å], tetragonal $Ni_{5.63}SnSe_2$ [space group: $I4/mmm$, lattice parameters: a = 3.690 (1) Å and c = 18. 695 (1) Å] are also shown. (b) XPS peak comparison of Sn in Ag, 1st Ni, 2nd Ni, and SnSe layers. Detailed phase identification results of Sn XPS peaks in (c) 1st Ni layer and (d) 2nd Ni layer (Color figure online).

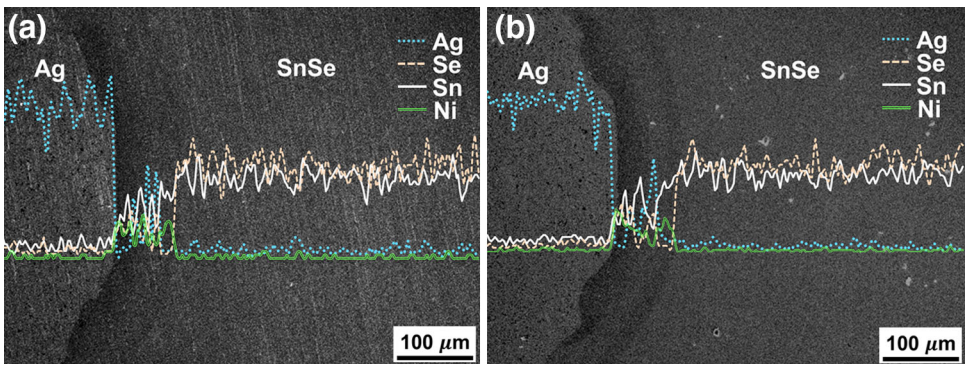

Fig. 7. EDS line scanning comparison of Ag/Ni bilayer metallization structures on SnSe (a) Before and (b) After high-temperature heat treatment at 723 K for 10 h.

greater variety of engineering approaches, than would direct modification of the thermoelectric interface, and might provide ultralow specific-contact resistivity metallization.

The SEM image of the Ni/SnSe interface layer in Fig. 5 confirms a unique columnar phase formation at the interface between SnSe and the 2nd Ni layer. To mimic the phase formation in the resultant Ni

functional layers; Ag, Ni, and SnSe powders were homogenously mixed; then heat treated under the same conditions as for the SnSe metallization for XRD analysis shown in Fig. 6a. The Rietveld refinement result of the aforementioned mixture (determined using Fullprof software[26]) shows the formation of Ni-Sn intermetallic phases (Ni_3Sn and Ni_3Sn_2) and $Ni_{5.63}SnSe_2$ along with Ni and Ag metals. The reliability factors of the refinements, R_p, R_{wp}, R_{exp}, and χ^2 were 3.47%, 4.86%, 3.06%, and 2.52. The obtained weight fraction values of Ag, Ni, Ni_3Sn, Ni_3Sn_2, and $Ni_{5.63}SnSe_2$ were 22.2 ± 0.5%, 2.7 ± 0.1%, 25.8 ± 0.5%, 0.4 ± 0.1%, and 48.9 ± 0.5%. The formation of these phases in the metallization layer was further investigated using Sn XPS in Fig. 6b, c, and d. Detailed study of the XPS peak of Sn in the 1st Ni layer, revealed two major peaks (of $Ni_{5.63}SnSe_2$ and SnSe), along with a small portion of Ni-Sn intermetallic phases (Ni_3Sn and Ni_3Sn_2), as shown in Fig. 6c.[27,28] These three peaks also appeared in the 2nd Ni layer (Fig. 6d) with slightly different ratios of each phase (compared to the results in Fig. 6c). The combined XPS and XRD results confirm that the functional Ni layer is reacted with SnSe to form columnar Ni-Sn phases and $Ni_{5.63}SnSe_2$, which suppressed Sn diffusion into the Ag layer without deterioration of the electrical contact characteristics.

The high-temperature stability of the proposed Ag/Ni bilayer structure has been initially tested and the results are shown in Fig. 7. The metallized SnSe thermoelectric leg was heat treated at 723 K (the expected average hot-side operation temperature is between 673 and 773 K) for 10 h in Ar gas. The EDS line scanning comparison in Fig. 7 shows that there was no apparent difference between the profiles of the elements before or after the high-temperature treatment. The Sn profile in Fig. 7b clearly showed that the proposed Ag/Ni bilayer effectively prevented Sn diffusion into the Ag layer even after 10 h continuous heat treatment at 723 K. The thicknesses of 1st and 2nd Ni layers were the same before and after the heat treatment. The initial high-temperature test in Fig. 7 showed that the proposed Ag/Ni bilayer metallization structure was stable under the expected high-temperature operating condition. More detailed investigation on the phases in the 1st and 2nd Ni layers, and long-term stability tests for highly efficient and reliable SnSe thermoelectric module metallization are the subjects of future work.

CONCLUSIONS

In this paper, the metallization results are reported for thermoelectric SnSe with a Ag/Ni bilayer structure. A single Ag metallization layer could not provide a reliable metallization interface with the SnSe thermoelectric leg due to a problem with Sn diffusion into the Ag layer, and resulting relatively high contact resistivity. A single Ni metallization layer resulted in surficial cracks and failure to establish a robust contact on the thermoelectric SnSe surface. The proposed Ag/Ni bilayer clearly prevented Sn diffusion into the Ag layer as well as mechanical cracks. Detailed investigation showed that Ni-Sn phases (Ni_3Sn and Ni_3Sn_2) and $Ni_{5.63}SnSe_2$, in particular, made a unique columnar microstructure in the metallization layers. The Ag/Ni bilayer metallization showed low electrical specific-contact resistivity (5.32×10^{-4} Ω cm^2); ten times lower than with single Ag metallization. The initial high-temperature test at 723 K showed stable characteristics of the Ag/Ni bilayer metallization structure, and showed that Sn is distinctly prevented for penetration into the Ag layer. More detailed and extended investigation on the long-term stability of the proposed Ag/Ni bilayer structure should be followed up in future work. Based on the results from this metallization investigation of polycrystalline SnSe, and assuming further modification of the electrical specific-contact resistivity, the result could be development of a practical, high-conversion-efficiency SnSe thermoelectric module.

ACKNOWLEDGEMENTS

This work was conducted under the framework of the Research and Development Program of the Korea Institute of Energy Research (KIER, B6-2448). This research was also supported by the National Research Foundation of Korea (NRF) Grant funded by the Korean Government (MSIP) (NRF-2015R1A5A1036133).

REFERENCES

1. S.B. Riffat and X. Ma, *Appl. Therm. Eng.* 23, 913 (2003).
2. X. Niu, J. Yu, and S. Wang, *J. Power Sources* 188, 621 (2009).
3. C. Lertsatitthanakorn, *Bioresour. Technol.* 98, 1670 (2007).
4. X.F. Zheng, Y.Y. Yan, and K. Simpson, *Appl. Therm. Eng.* 53, 305 (2013).
5. C. Hadjistassou, E. Kyriakides, and J. Georgiou, *Energy Convers. Manag.* 66, 165 (2013).
6. A. Muto, J. Yang, B. Poudel, Z. Ren, and G. Chen, *Adv. Energy Mater.* 3, 245 (2013).
7. M. Gürth, G. Rogl, V.V. Romaka, A. Grytsiv, E. Bauer, and P. Rogl, *Acta Mater.* 104, 210 (2016).
8. G. Rogl, A. Grytsiv, K. Yubuta, S. Puchegger, E. Bauer, C. Raju, R.C. Mallik, and P. Rogl, *Acta Mater.* 95, 201 (2015).
9. X. Hu, P. Jood, M. Ohta, M. Kunii, K. Nagase, H. Nishiate, M.G. Kanatzidis, and A. Yamamoto, *Energy Environ. Sci.* 9, 517 (2016).
10. J. Zhao, Z. Liu, J. Reid, K. Takarabe, T. Iida, B. Wang, U. Yoshiya, and J.S. Tse, *J. Mater. Chem. A* 3, 19774 (2015).
11. L.D. Zhao, S.H. Lo, Y. Zhang, H. Sun, G. Tan, C. Uher, C. Wolverton, V.P. Dravid, and M.G. Kanatzidis, *Nature* 508, 373 (2014).
12. R. Bjørk, *J. Electron. Mater.* 44, 2869 (2015).
13. Y. Kim, G. Yoon, and S.H. Park, *Exp. Mech.* 56, 861 (2016).
14. C.C. Li, F. Drymiotis, L.L. Liao, H.T. Hung, J.H. Ke, C.K. Liu, C.R. Kao, and G.J. Snyder, *J. Mater. Chem. C* 3, 10590 (2015).
15. C.C. Li, F. Drymiotis, L.L. Liao, M.J. Dai, C.K. Liu, C.L. Chen, Y.Y. Chen, C.R. Kao, and G.J. Snyder, *Energy Convers. Manag.* 98, 134 (2015).
16. F.R. Sie, C.S. Hwang, Y.H. Tang, C.H. Kuo, Y.W. Chou, C.H. Yeh, H.Y. Ho, Y.L. Lin, and C.H. Lan, *J. Electron. Mater.* 44, 1450 (2015).

17. K.T. Wojciechowski, R. Zybala, and R. Mania, *Microelectron. Reliab.* 51, 1198 (2011).
18. V. Semenyuk and O. Antonenko, in *Proceedings of the 5th European Conference on Thermoelectrics* (2007).
19. H.H. Hsu, C.H. Cheng, S.H. Chiou, C.H. Huang, C.M. Liu, Y.L. Lin, W.H. Chao, P.H. Yang, C.Y. Chang, and C.P. Cheng, *J. Alloys Compd.* 588, 633 (2014).
20. C.L. Yang, H.J. Lai, J.D. Hwang, and T.H. Chuang, *J. Electron. Mater.* 42, 359 (2013).
21. L. Shi, X. Huang, M. Gu, and L. Chen, *Surf. Coat. Technol.* 285, 312 (2016).
22. D. Zhao, H. Geng, and X. Teng, *J. Alloys Compd.* 517, 198 (2012).
23. J.R. Sarvador, J.Y. Cho, Z. Ye, J.E. Moczygemba, A.J. Thompson, J.W. Sharp, J.D. Konig, R. Maloney, T. Thompson, J. Sakamoto, H. Wang, A.A. Wereszczak, and G.P. Meisner, *J. Electron. Mater.* 42, 7 (2013).
24. J. Graff, J. He, and T.M. Tritt, *Inorganics* 2, 168 (2014).
25. C. Fu, T. Zhu, Y. Liu, H. Xie, and X. Zhao, *Energy Environ. Sci.* 8, 216 (2015).
26. J. Rodríguez-Carvajal, Commission on powder diffraction (IUCr). *Newsletter* 26, 12 (2001).
27. A. Onda, T. Komatsu, and T. Yashima, *Phys. Chem. Chem. Phys.* 2, 2999 (2000).
28. S. Badrinarayanan, A.B. Mandale, V.G. Gunjikar, and A.P.B. Sinha, *J. Mater. Sci.* 21, 3333 (1986).